Kinetics and Motional Dynamics of Spin-Labeled Yeast Iso-1-cytochrome *c*: 1. Stopped-Flow Electron Paramagnetic Resonance as a Probe for Protein Folding/Unfolding of the C-Terminal Helix Spin-Labeled at Cysteine 102[†]

Kunbin Qu,[‡] Jeffrey L. Vaughn,[§] Andrzej Sienkiewicz,[||] Charles P. Scholes,[⊥] and Jacquelyn S. Fetrow*[,§]

Departments of Chemistry, Physics, and Biological Sciences, Center for Biophysics and Biochemistry, State University of New York at Albany, Albany, New York 12222, and Institute of Physics of the Polish Academy of Sciences, Al. Lotnikov 32/46, 02668 Warsaw, Poland

Received August 26, 1996; Revised Manuscript Received January 7, 1997[⊗]

ABSTRACT: The kinetics of chemically induced folding and unfolding processes in spin-labeled yeast iso-1-cytochrome *c* were measured by stopped-flow electron paramagnetic resonance (EPR). Stopped-flow EPR, based on a new dielectric resonator structure [Sienkiewicz, A., Qu, K., & Scholes, C. P. (1994) *Rev. Sci. Instrum. 65*, 68−74], gives a new temporal component to probing nanosecond molecular tumbling motions that are modulated by macromolecular processes requiring time resolution of milliseconds to seconds. The stopped-flow EPR technique presented in this work is a kinetic technique that has not been previously used with such a time resolution on spin-labeled systems, and it has the potential for application to numerous spin-labeled sites in this and other proteins. The cysteine-specific spin-label, methanethiosulfonate spin-label (MTSSL), was attached to yeast iso-1-cytochrome *c* at the single naturally occurring cysteine[102], and the emphasis for this work was on this disulfide-attached spin-labeled prototype. This probe has the advantage of reflecting the protein tertiary fold, as shown by recent, systematic site-directed spin labeling of T4 lysozyme [Mchaourab, H. S. Lietzow, M. A., Hideg, K., & Hubbell, W. L. (1996) *Biochemistry 35*, 7692−7704], and protein backbone dynamics, as also shown by model peptide studies [Todd, A. P., & Millhauser, G. L. (1991) *Biochemistry 30*, 5515−5523]. The C-terminal cytochrome *c* helix where the label is attached is thought to be critical in the initial steps of protein folding and unfolding. Stopped-flow EPR resolved the monoexponential, guanidinium-induced unfolding process at pH 6.5 with an ∼20 ms time constant; this experiment required less than 150 μL of 80 μM spin-labeled protein. We observed an ∼50-fold decrease of this unfolding time from the 1 s range to the 20 ms time range as the guanidinium denaturant concentration was increased from 0.6 to 2.0 M. The more complex refolding kinetics of our labeled cytochrome were studied by stopped-flow EPR at pH 5.0 and 6.5. The spin probe showed a fast kinetic process compatible with the time range over which hydrogen/deuterium amide protection indicates helix formation; this process was monoexponential at pH 5.0. At pH 6.5, there was evidence of an additional slower kinetic phase resolved by stopped-flow EPR and by heme-ligation-sensitive UV−Vis that indicated a slower folding where heme misligation may be involved. Since the disulfide-attached probe has reported folding and backbone dynamics in other systems, the implication is that our kinetic experiments were directly sensing events of the C-terminal helix formation and possibly the N- and C-terminal helical interaction. The cysteine-labeled protein was also studied under equilibrium conditions to characterize probe mobility and the effect of the probe on protein thermodynamics. The difference in spin probe mobility between folded and denatured protein was marked, and in the folded protein, the motion of the probe was anisotropically restricted. The motion of the attached nitroxide in the folded protein appears to be restricted about the carbon and sulfur bonds which tether it to the cysteine. The original point of cysteine sulfur attachment is ∼11 Å from the heme iron within the C-terminal helix near its interface with the N-terminal helix, but the low-temperature EPR spin probe line width showed that the probe lies more distant (>15 Å) from the heme iron. By all physical evidence, the protein labeled at cysteine[102] folded, but the spin probe in this prototype system perturbed packing which lowered the thermal melting temperature, the free energy of folding, the guanidinium concentration at the midpoint of the unfolding transition, the *m* parameter of the denaturant, and the helical CD signature. This study prepares the way for study of protein folding/unfolding kinetics using EPR spectroscopy of spin-labels placed at specific cysteine-mutated sites within the protein.

The structure, dynamics, and conformation of small proteins as they undergo folding and unfolding are a major quest in modern structural biology. For the purpose of probing folding and unfolding, we have chosen the protein iso-1-cytochrome *c* from the yeast *Saccharomyces cerevisiae*. The crystal structure of native iso-1-cyt *c*[1] (Figure 1A) and a number of its mutants have been solved (Berghuis et al.,

[†] These studies were partially supported by NIH Grants GM-44829 (J.S.F.) and GM-35103 (C.P.S.) and by the Maria Sklodowska Curie U.S.-Polish Joint Fund II PAN/NIST-94-203 (A.S.). Acknowledgment is made to the Donors of the Petroleum Research Fund, administered by the American Chemical Society, for partial support of this research (29658-AC4 to J.S.F. and C.P.S.).

* Author to whom correspondence should be addressed: Department of Biological Sciences, State University of New York at Albany, 1400 Washington Ave., Albany, NY 12222. Phone: 518-442-4389. Fax: 518-442-4767. E-mail: jacque@isadora.albany.edu.

[‡] Department of Physics, State University of New York at Albany.

[§] Department of Biological Sciences, State University of New York at Albany.

[||] Institute of Physics of the Polish Academy of Sciences.

[⊥] Department of Chemistry, State University of New York at Albany.

[⊗] Abstract published in *Advance ACS Abstracts,* February 15, 1997.

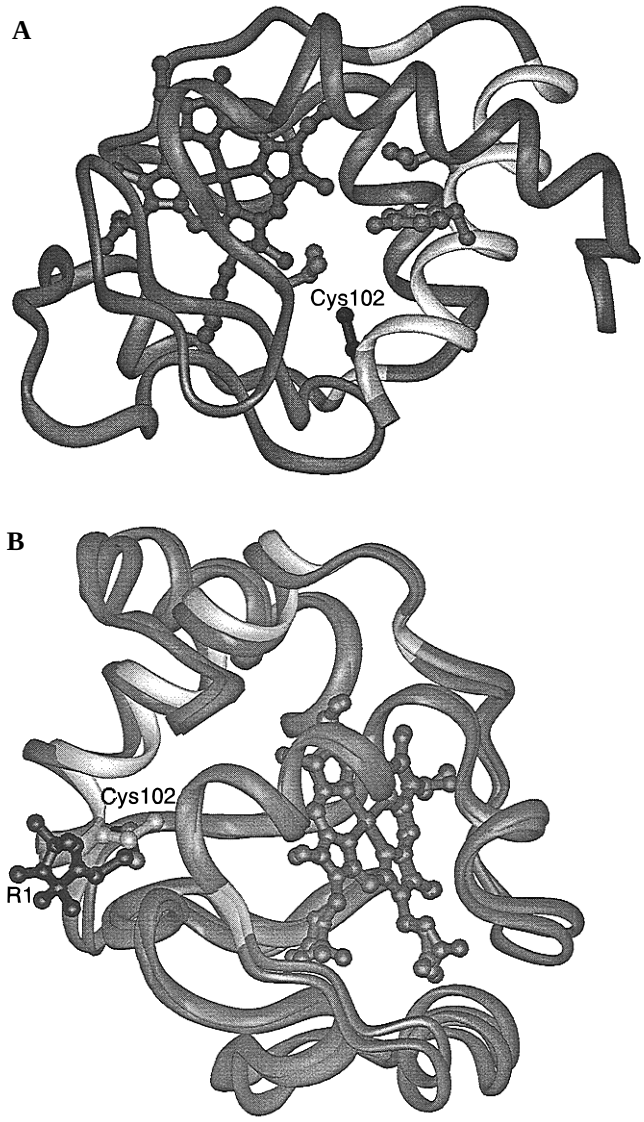

FIGURE 1: (A) Ribbon structure of native yeast iso-1-cytochrome *c* drawn from the energy-minimized structure (see Materials and Methods) based on the coordinates of Louie and Brayer (1990). The side chains of the Cys^{102}, Val^{20}, Leu^{94}, and Tyr^{97} are shown as they occupy the internal hydrophobic region about the C-terminal helix. The C-terminal helix is itself shown in light gray. (B) This figure compares the energy-minimized structures of native C102 and R1-labeled C102-SL where the heme groups were superimposed. The R1 label is shown in black ball and stick, the perturbed C-terminal helix of C102-SL in dark gray, and the unperturbed C-terminal helix of native C102 in light gray.

1994; Lo et al., 1995; Louie & Brayer, 1990; Murphy et al., 1992). The crystal structures of several other prokaryotic (Matsuura et al., 1982; Timkovich & Dickerson, 1976) and eukaryotic cytochromes (Ochi et al., 1983; Takano & Dickerson, 1980; Bushnell et al., 1990; Berghuis & Brayer, 1992) are also known. The protein is highly amenable to spectroscopic methods, and the protein is easily genetically manipulated so that a large body of data from site-directed mutagenesis studies is available (Sherman et al., 1974; Hampsey et al., 1986; Auld & Pielak, 1991; Betz & Pielak, 1992; Fredericks & Pielak, 1993; Marmorino & Pielak, 1995; Pielak et al., 1995; Fetrow et al., 1997). The thermodynamic properties of the protein are easy to study experimentally [see, for example, Cohen and Pielak (1994)]. The effect of mutations can be analyzed both *in vitro* and *in vivo* (Cottrell et al., 1975; Schweingruber et al., 1977; Linske-O'Connell et al., 1995; Fetrow et al., 1989, 1997).

Cytochrome *c*, particularly the readily available horse heart variety, has been a central figure in elucidating the kinetics of protein folding and unfolding. The unfolding induced by denaturant appears to be a single global event (Schmid, 1992; Colón et al., 1996). The refolding kinetics for horse heart cyt *c* variants have been deconvoluted into three observable exponential phases at neutral pH (Colón et al., 1996): a fast phase in the 5−100 ms range, an intermediate phase in the 0.5−1 s range, and a minor slow phase in the 5−25 s range. The fast 5−100 ms phase reflects the formation of a partially folded intermediate due to association of the N- and C-terminal helices; it is this phase that has also been a major focus of deuterium/hydrogen exchange of amide protons on the N- and C-terminal helices (Roder et al., 1988; Elöve et al., 1992, 1994). On the same time scale, there is a rapid contraction in the unfolded structure, as shown by heme-induced tryptophan fluorescence quenching (Tsong, 1976) and by the secondary helical structure as sensed by CD (Elöve et al., 1992). The intermediate phase can be attributed to a state with improper heme−histidine ligation that will convert into the native state following dissociation of the non-native histidine iron ligand (Elöve et al., 1992, 1994; Sosnick et al., 1994). The slow phase is most likely due to cis/trans isomerization of prolyl peptide bonds. When refolding is carried out at pH ∼5 rather than at pH 6.5, the misfolding is eliminated so that only the faster kinetic steps remain (Elöve et al., 1994; Sosnick et al., 1994). The foregoing kinetics were determined from rapid-mix and/or stopped-flow techniques. Some changes occurred within the dead time, too early to be explicitly measured. What was initially called a "burst" stage (≤5 ms) of folding has suggested formation of a compact state with incompletely defined helical structure (Creighton, 1994; Colón et al., 1996; Sosnick et al., 1996). Recently reported laser-triggered methods of promoting folding through change of heme ligation (Jones et al., 1993) or redox state (Pascher et al., 1996) suggest that some aspects of the burst attributed to hydrophobic collapse start in submilliseconds.

Previously, spectroscopic probes of folding have primarily focused on the following: (1) a chromophore such as the heme which reports heme-centered ligation events or such as the sole tryptophan whose fluorescence is generally sensitive to iron−tryptophan separation (via a $1/r^6$ dependence), (2) the general secondary structural conformation as reported by CD, and (3) the particular event of proton exchange which, for hydrogen-bonded amide protons, provides an indication of a formed, stable helix or other hydrogen-bonded structure. Spin-label EPR spectroscopy probes nanosecond dynamics of a protein, and our goal was

[1] Abbreviations: EPR, electron paramagnetic resonance; MTSSL, methanethiosulfonate spin-label; R1, disulfide-linked nitroxide spin-label that results from the reaction of MTSSL and cysteine; GdnHCl, guanidinium hydrochloride (Sigma, 99.5 % ultrapure); CD, circular dichroism; UV−Vis, ultraviolet−visible spectroscopy; LGR, loop gap resonator; DR, dielectric resonator; CW, continuous wave as opposed to transient; ptp, peak-to-peak; T_m, temperature at the midpoint of the thermal melting transition; C_m, GdnHCl concentration at the midpoint of the GdnHCl unfolding transition expressed in molarity; iso-1-cyt *c*, yeast iso-1-cytochrome *c*; C102, unlabeled native iso-1-cyt *c*; C102T, iso-1-cyt *c* with a $Cys^{102} \rightarrow Thr^{102}$ mutation made for the purpose of preventing slow dimerization; C102-SL, iso-1-cyt *c* spin-labeled with R1 at its naturally occurring Cys^{102}.

to apply it to the conformational changes on the millisecond or longer time scale of protein folding/unfolding.

Spin labeling has been available as a probe for molecular motion for a generation [see, e.g., Berliner (1975)]. A major advantage of the standard absorption derivative ($d\chi''/dH$) spin-label EPR signal is the fact that its line shape is sensitive to dynamic tumbling processes on the 0.01−10 ns time scale. This is a time scale that stretches from the tumbling time of a globular protein larger than cytochrome *c* to rapid tumbling of a completely mobile small nitroxide. In application to the membrane-bound colicin (Todd et al., 1989) and bacteriorhodopsin (Altenbach et al., 1989, 1990), the powerful technique of site-directed spin labeling was used. In this technique, specific amino acids were mutated to cysteine, and a highly cysteine-specific probe called MTSSL (methanethiosulfonate spin-label) was attached to give a disulfide-linked nitroxide called R1 by Mchaourab et al. (1996) (see the structure). The motion of R1 distinguished between

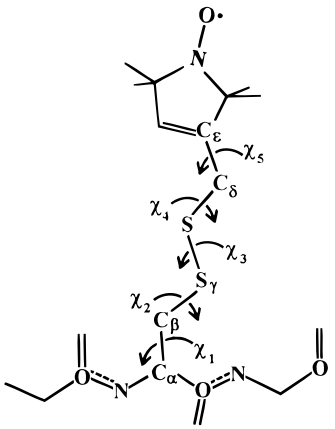

specific amino acid attachment sites in helical regions, in amphoteric regions at lipid−aqueous interfaces, in transmembrane spanning regions, and in solvent-exposed regions. When MTSSL was incorporated into rhodopsin (Farahbakash et al., 1993) or bacteriorhodopsin (Steinhoff et al., 1994), both of which undergo conformational changes upon absorption of light, the spin-label reported on the millisecond time scale a conformational change triggered by a laser pulse. So the spin label which is sensitive to motions on the nanosecond time scale *can* simultaneously report conformational changes on the millisecond time scale.

Millhauser and co-workers have used MTSSL attached to short model peptides to follow the variation of helix mobility at positions throughout the peptide and to follow the local and global dynamics of unfolding (Todd & Millhauser, 1991; Miick et al., 1991). In a recent application of site-directed spin labeling, over 30 site-directed cysteine labelings were systematically performed within T4 lysozyme, at solvent accessible positions on helices, at loops, at positions within internal hydrophobic regions, and at positions where tertiary interactions with other side chains were predicted (Mchaourab et al., 1996). The resultant disulfide-attached nitroxide chain, R1, faithfully reflected the protein fold at all sites investigated, and the mobility of the nitroxide side chain was determined by tertiary interactions and, especially for labels on α-helices, by internal backbone dynamics. The conclusion from numerous MTSSL labelings followed by systematic changes in the structure of the probe and its tether was that the segment of R1 stretching from the cysteine C_α through the attached S−S bond is immobile on the EPR time scale, and the motions about the subsequent S−C_δ and C_δ−C_ϵ bonds (see the structure) that attach the nitroxide ring to the disulfide are restricted, anisotropic, and highly sensitive to the backbone motions emanating from the cysteine where the spin-label attachment was made. The MTSSL in the attached R1 form is thus an effective reporter of backbone motions (Mchaourab et al., 1996).

EPR spectroscopy and stopped-flow methods have both been available for four decades, but their marriage has not been consummated until now. The first stopped-flow EPR systems, based on a flow-flat cell insert to a standard X-band TE_{102} EPR cavity, were highly vibration sensitive, would not readily adapt to sub-100 ms kinetic measurements, and used copious amounts of reactant (1 mL/shot). Carlsson et al. (1975) used such a flow-flat cell coupled to a 100 ms dead time mixer for observing refolding of carbonic anhydrase, and the indication was that the folding occurred in something less than 100 ms. In the 1980s, the technology of small resonant structures emerged; the first was the loop gap resonator (LGR) of Froncisz and Hyde (1982). A novel LGR design for continuous and stopped-flow EPR was presented which provided high sensitivity on microliter sample volumes (Hubbell et al., 1987). An Update Instrument (Madison, WI) delivery system reproducibly injected small liquid volumes through a high-efficiency Wiskind grid mixer. The dead volumes and flow velocities would, in principle, enable kinetic behavior to be detected on a millisecond time scale previously reserved for optically detected stopped flow. With this device, the course of colicin's membrane insertion on the time scale of seconds at specific spin-labeled positions was monitored (Shin et al., 1993). Because of incomplete isolation of its microwave electric and microwave magnetic fields, the LGR is inherently sensitive to flow and stopped-flow-induced noise originating in the high-dielectric aqueous sample. Sienkiewicz et al. (1994) developed an altogether different miniature resonant structure to mate with the pre-existing Update rapid-mix system, and this structure was based on the inexpensive, commercially available ceramic dielectric resonator (DR). In contrast to the LGR, the electric part of the microwave field in the DR is well isolated from the aqueous, high-dielectric, lossy sample, while the EPR-active microwave magnetic field is still concentrated on the sample. The DR is thus insensitive to stopped-flow-induced noise transients (glitches) so that kinetic transients occurring over less than 30 ms may be resolved [see Figure 6 of Sienkiewicz et al. (1994)]. The DR provides the technical basis for the stopped-flow EPR reported here.

The primary purpose of the work reported here was to test the application of stopped-flow EPR to protein folding by following the folding/unfolding kinetics of yeast iso-1-cytochrome *c* as reported by R1 attached at the naturally occurring Cys^{102} (Figure 1) and as obtained with the first biological application of our DR-based rapid-mix stopped-flow EPR. For the prerequisite background, we characterized this spin-labeled derivative (C102-SL) by EPR to delineate the probe motion under folding and unfolding conditions. We also used a battery of spectroscopic techniques which characterized the structural and thermodynamic perturbations on the protein due to the probe.

MATERIALS AND METHODS

Preparations

Yeast Strains, Mutagenesis, Protein Purification, and Nomenclature. The strains, mutagenesis, and protein purification methods used for this study are as described elsewhere (Murphy et al., 1993; Mulligan-Pullyblank et al., 1996; Fetrow et al., 1997). Unlabeled, native iso-1-cyt *c* is called C102. (Iso-1-cyt *c* has a five-residue N-terminal extension; thus, we follow the convention of numbering the protein from −5 to 103 on the basis of its sequence alignment to other eukaryotic cytochromes *c*.) Protein that has been specifically labeled with MTSSL at residue 102 to yield the attached R1 group is called C102-SL; the position of labeling is indicated in Figure 1B. Thermodynamic control experiments were carried out with C102 and with C102T, a protein containing the mutation $Cys^{102} \rightarrow Thr^{102}$, designed to prevent cysteine dimerization (Cutler et al., 1987).

Protein Spin Labeling. Methanethiosulfonate spin label (MTSSL; Reanal, Budapest, Hungary) and free cysteine react with high specificity to form disulfide-linked R1 (Todd et al., 1989). For these experiments, a slight stoichiometric excess of spin-label solution [MTSSL dissolved in 50% 0.01 M $NaPO_4$ (pH 7.0) and 50% ethanol] was added to the protein solution which had previously been dissolved or dialyzed into 0.01 M phosphate buffer at pH 7.0. The combined solution was reacted at room temperature for 40 min with occasional vortexing. Unreacted MTSSL was removed by chromatography upon Sephadex G-25 resin (Pharmacia). The eluant was dialyzed in the cold overnight against the appropriate buffer to achieve the desired pH value. The resulting product yielded a single peak, whose retention time on a C18 reverse phase HPLC column was distinguishable from the peak for unreacted protein (data not shown).

Physical Methods

UV−Visible and CD Spectrophotometry. Denaturation experiments were monitored by the far-UV CD signal at 222 nm and the near-UV CD signal at 281.5 and 287.5 nm. These wavelengths monitor, respectively, temperature-dependent changes in the regular secondary structure (N- and C-terminal and 60's helices) and tertiary structure of the aromatic side chains in the heme region (Myer, 1985). The CD data were collected on an Aviv 62DS spectrometer fitted with a five-position, thermostated sample changer, and protein concentrations were approximately 6−7 μM. Temperature-dependent changes of the heme environment were also monitored with UV−Vis absorption spectroscopy at 280, 287, 360, 399, and 415 nm (Moore & Pettigrew, 1990). UV−Vis equilibrium data were collected on an SLM-Aminco DW2000 instrument fitted with a constant temperature cuvette holder connected to a Neslab water bath.

Standard EPR Spectroscopy. A Bruker ER-200 EPR spectrometer was fitted with a TE_{102} rectangular cavity, a variable-temperature EPR quartz flat cell (Wilmad), and variable-temperature accessories. Standard first-derivative absorption ($d\chi''/dH$) spectra, such as those shown in Figure 2, were collected. Temperatures higher than 273 K were controlled by a gas flow system in conjunction with Bruker's B-VT-1000 temperature controller, and these temperatures were calibrated in the 273−350 K range with a thermocouple directly attached to the in-cavity flat cell. The modulation amplitude was kept at 0.5 G to prevent unwanted line broadening. The power used was a nonsaturating 2 mW. The protein concentrations for standard EPR experiments were ∼30 μM. For cryogenic work at ∼10 K, a Helitran helium gas flow system was interfaced with a Scientific Instruments APD-E digital temperature indicator/controller. A Compaq 486 PC equipped with an IBM digital-to-analog converter and Scientific Sales Systems EW2.41A software collected both CW and kinetic EPR data.

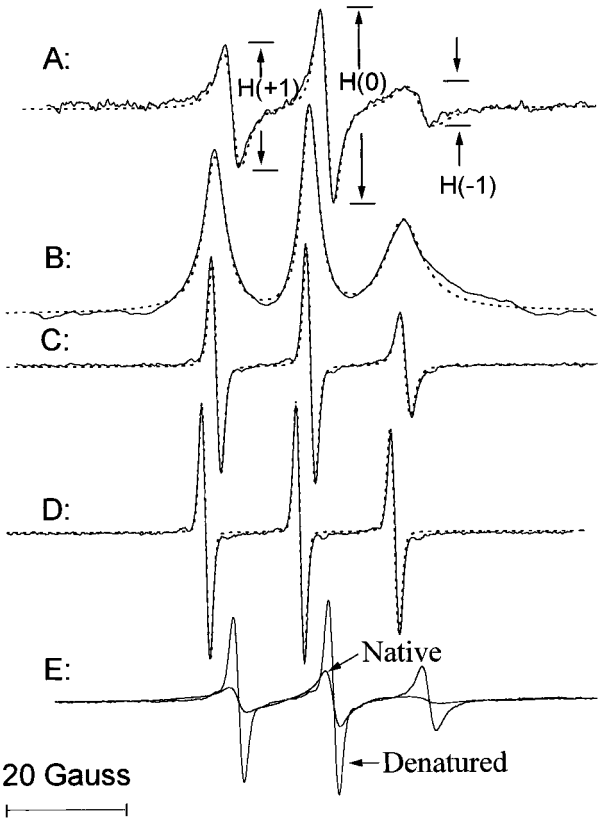

FIGURE 2: EPR spectra of spin-labeled yeast iso-1-cytochrome *c* in 0.1 M sodium acetate buffer at pH 5. Solid lines are experimental, and dotted lines are simulated (Schneider & Freed, 1989). (A) Folded protein at 15 °C. For simulation, the diffusion tensors were as follows: $d_{xy} = 6$ E07 and $d_{zz} = 2.3$ E08 which correspond to $\tau_\perp = 2.78$ ns and $\tau_\parallel = 0.72$ ns. The *y* axis is the axis of fast diffusion. (B) First integral of spectrum A. (C) Denatured protein in 2 M GdnHCl at 15 °C. For simulation, the diffusion tensors were as follows: $d_{xy} = d_{zz} = 2.8$ E08 which correspond to $\tau_{iso} = 0.35$ ns. (D) C102-SL at 75 °C. For simulation, the diffusion tensors were as follows: $d_{xy} = d_{zz} = 1.67$ E09 which correspond to $\tau_{iso} = 0.10$ ns. The *g* and *A* values were those which Todd and Millhauser (1991) took for MTSSL; viz., $A_{zz} = 35.7$ G, $A_{yy} = 6.23$ G, $A_{xx} = 6.23$ G, $g_{zz} = 2.0086$, $g_{yy} = 2.0066$, and $g_{xx} = 2.0032$. The fast-tumbling axis was close to the *y* tensor axis. The truncation parameters in the Schneider and Freed (1989) simulation are as follows: $L^e_{max} = 6$, $L^o_{max} = 3$, $K_{max} = 2$, $M_{max} = 2$, and $p^l = 2$. The number of Lanczos steps was 33. The intrinsic line width parameters are as follows: $W^{int}_0 = 0$ and $W^{int}_2 = 0$. The simulations were convoluted with a Gaussian line width of 1.2 G between derivative extrema to simulate inhomogeneous proton broadening from methyl protons. (E) Overlay of folded C102-SL and unfolded C102-SL in 1.6 M GdnHCl, at pH 6.5 and 2 °C to show the relative intensity of EPR signals taken in the small tube in the DR from the same 40 μM concentration of folded and unfolded protein.

Rapid-Mix, Stopped-Flow EPR. The dielectric resonator-based stopped-flow system is described in Sienkiewicz et al. (1994). The $TE_{0,1,\delta}$ DR resonant structure provides a 30-fold sensitivity increase over a standard EPR cavity for the

~2 μL active sample volume. As interfaced to an Update Instrument, Inc. (Madison, WI), rapid-mix Wiskind grid mixer immediately adjacent to the resonator, the system has a dead volume of 5 μL. Experiments were run primarily with a programed ram speed of 1 cm/s, a reactant flow rate of 660 μL/s, and a dead time of ~8 ms; a number of experiments were also run with a reactant flow rate of 1320 μL/s and a dead time of ~4 ms. Triggering of data collection was provided by a pulse from the controller. Coolant (provided by a Neslab model RTE-9B refrigerated circulating bath) was flowed about storage syringes and liquid delivery tubes, and the mixer body was additionally cooled by a Cold Air Gun (ITW Vortec, DoALL Part 013901). The temperature was monitored by a thermocouple mounted on the resonator body, and the internal temperature of the dielectric resonator was internally checked via a temperature sensitive spin-label signal that had been previously calibrated in the CW EPR system above. The majority of stopped-flow EPR experiments were carried out at 2 °C, where folding/unfolding kinetics were observable over a wide range of denaturant and pH conditions and where the temperature stability, control, and precision (±1 °C) within the critical dielectric resonator volume were optimal.

Stopped-Flow UV−Vis. Complementary stopped-flow measurements monitored by visible detection of the heme absorption were performed by an Aminco-Morrow stopped-flow attachment coupled to a retrofitted DW-2 UV−Vis spectrophotometer [the original by SLM Instruments (Urbana, IL), with retrofit by On Line Instrument Systems (OLIS) Inc. (Jefferson, GA)]. This stopped-flow device has a mixer with a 1970s design; we were warned about its potential for Schlieren mixing artifacts due to incomplete mixing of dilute buffer and concentrated GdnHCl (R. Hansen, Update Instrument, Inc., personal communication). We have observed such optical artifacts over a time of ~5 ms after mixing, and we therefore do not attempt to estimate with our optical stopped-flow system the optical absorption change during flow. The temperature was controlled by coolant flowing from the Neslab refrigerated circulating bath through ports in the stopped-flow attachment, and the temperature was monitored by a thermocouple mounted on the mixer. Kinetic data collection software and kinetic fitting software were provided by OLIS.

Methods of Analysis

Empirical EPR Line Shape Analysis. Tumbling, as it modulates the anisotropic hyperfine and Zeeman interactions, causes the three hyperfine lines of the $I =$ one ^{14}N nucleus to vary differently in amplitude and line width. As a spin-label becomes more mobile, there will be a relative increase in outer derivative ($M = \pm 1$) peak heights with respect to the central ($M = 0$) peak. The T_2 for these three lines can be represented by

$$[T_2(M)]^{-1} = A + BM + CM^2 \qquad (1)$$

($M = +1$, 0, and -1, corresponding to left, central, and right EPR lines, respectively). The A term is common to all three EPR lines, but B and C can be determined from relative intensities and line widths of the three EPR lines after Marsh (1989, pp 259−262) and Todd and Millhauser (1991, p 5517). Details of the methods for determining B and C and their relation to tumbling correlation times are provided and discussed in the Supporting Information. If the tumbling is isotropic, B and C yield the same isotropic correlation time, τ_{iso}.[2] If tumbling is anisotropic, B and C will yield two different correlation times, $\tau_{||}$ and $\tau_{\perp}$, where $\tau_{||}$ is the shorter tumbling time about a diffusion axis that allows faster tumbling and $\tau_{\perp}$ is the longer tumbling time perpendicular to this axis. A $|C/B|$ ratio not equal to 1 is evidence for anisotropy of tumbling.

EPR Line Shape Simulation. EPR line shape simulation was carried out using the general software package of Schneider and Freed (1989). This program solves the stochastic Liouville equation and calculates the EPR line shape under conditions where one is not restricted to correlation times of less than 1−2 ns. Details are discussed in the Supporting Information.

Protein Denaturation. Thermal and guanidinium hydrochloride denaturations of C102 and C102-SL were done to determine how much the spin-label perturbed the protein stability. Protein was dissolved or dialyzed into 100 mM sodium acetate buffer at pH 5.0, diluted to a final concentration of about 15 μM, and placed in a 0.1 cm quartz cuvette. Protein concentrations were determined by absorption spectroscopy at 410 nm on an SLM-Aminco UV−visible DW2000 spectrophotometer using an extinction coefficient of 106.1×10^3 L M^{-1} cm^{-1} (Margoliash & Frohwirt, 1958). Changes in ellipticity with respect to temperature or denaturant concentration were monitored using an Aviv Model 62 DS circular dichroism spectropolarimeter fitted with a five-cell thermoelectric cuvette changer. CD data at 222 nm were collected by computer using a 1 min equilibration time and a 30 s averaging time.

For thermal denaturations, the data were fit by nonlinear least-squares analysis using the method of Cohen and Pielak (1994), which is based on the modified integrated Gibbs−Helmholtz equation of Elwell and Schellman (1977). This equation relates the temperature to the mean residue ellipticity using the slopes and intercepts of the baselines, ΔH_m, and T_m as fitting parameters. In these calculations, ΔC_p was not fit to the equations but was set as a constant at 1.37 kcal mol^{-1} K^{-1}, which is the value determined by Cohen and Pielak (1994) for wild type C102T iso-1-cytochrome *c*.

Both of the methods for fitting chemical or thermal denaturation data are fits to an assumed two-state denaturation process (see also footnote 5) where a denatured fraction of the protein, f_D, has a set of spectral characteristics different from that of the native fraction ($1 - f_D$). Equilibrium melting of cytochrome *c* was well fit to a two-state denaturation process (Cohen & Pielak, 1994) even though, as is often the case (Schmid, 1992), the kinetic evidence shows that folding is more complex. Guanidinium denaturations were done at 5 °C so that a clear baseline for folded C102-SL could be

[2] A Stokes−Einstein relation, $\tau = V_L\eta/(KT)$, will relate the rotational correlation time to what Todd and Millhauser (1991) call the local tumbling volume, V_L. This is a volume construed as the portion of the attached peptide that in effect reorients with the spin-label. Approximating iso-1-cyt *c* as a sphere with a radius of 15 Å, we estimate its entire tumbling volume, V_L, as 14 000 Å^3, and when solvent viscosity ~ 1.1 cP and $T = 288$ K, we estimate its tumbling correlation time at 4 ns. In thermally or GdnHCl-denatured protein, the local tumbling volume was only about 1500 Å^3. This volume is somewhat larger than the five-member nitroxide ring volume *per se* and undoubtedly demonstrates that there is an additional volume of nearby denatured protein which reorients with the probe as they move in solution.

obtained. For these experiments, the mean residue ellipticity at various guanidinium hydrochloride concentrations was fit by nonlinear least-squares analysis to the equation of Santoro and Bolen (1988) [see also Pace (1986) and Pace et al. 1989)]. This equation relates the denaturant concentration to the mean residue ellipticity using the slopes and intercepts of the baselines, ΔG_{H_2O} (which is the free energy of unfolding in the absence of GdnHCl), and the *m* parameter as fitting parameters. The values reported, ΔG_{H_2O} and the *m* parameter, are the *y* intercept and the slope, respectively, of a plot of denaturant concentration versus free energy of unfolding, where

$$\Delta G = \Delta G_{H_2O} - m[\text{GdnHCl}] \quad (2)$$

Chemical and thermal reversibility of unfolding was demonstrated for C102 and C102-SL to provide justification for using equilibrium equations to evaluate thermodynamic values. In GdnHCl denaturation experiments, the native secondary structure content of C102 and C102-SL was fully recovered after dilution into lower denaturant concentrations. When denatured to 65 °C for C102 and 52 °C for C102-SL (at least 5 °C beyond the unfolding transition zone) for 15 min and then rapidly cooled to 5 °C, both variants refolded to their native secondary structure (data not shown). Thermal and chemical denaturation of C102-SL monitored by EPR spectroscopy showed similar reversibility.

An empirically useful measure of thermal or chemical denaturations was the $H(-1)/H(0)$ ratio where $H(-1)$ and $H(0)$ are the peak-to-peak derivative heights of the high-field and central EPR features, respectively, as shown in Figure 2A. The empirical $H(-1)/H(0)$ melting presentation could be analyzed by a nonlinear least-squares fitting routine. However, the $H(-1)/H(0)$ ratio need not depend in a straightforward way upon the fraction (f_D) of protein that is unfolded and the fraction [$(1 - f_D) = f_N$] of protein that is folded, since both $H(-1)$ and $H(0)$ depend on these fractions. As outlined in the Supporting Information, we used our own least-squares routine to estimate more rigorously f_D values from EPR which are overlaid in Figure 4A with corresponding values from CD.

Sulfide-Linked Spin-Label R1 Incorporated via Molecular Mechanics into Iso-1-cytochrome c. Structures of the spin-label attached by disulfide to Cys^{102} were examined by molecular modeling techniques using the Biosym Technologies software package (San Diego, CA). MTSSL itself was first built using the Builder module, modeling the oxygen on the nitroxide as a hydroxyl. This molecule was attached to the yeast iso-1-cyt *c* through a disulfide bond to Cys^{102}. The nitroxide side chain attached in this manner pointed into the interior of the protein (as the side chain of Cys^{102} does in Figure 1), and at that point, it sterically interfered with other protein side chains. Cryogenic-temperature EPR line shape information indicated that the spin-label was further away from the heme than 11 Å, which was its original point of attachment. The computer model was examined for ways to move the sulfide-linked nitroxide with minimal perturbation of the protein. We found that this could easily be accomplished by simple rotation around the χ_1 and χ_2 side chain dihedral angles of R1 (see the structure in the introductory section for χ_1 and χ_2). The resulting model was then energy minimized to remove gross atomic overlaps. Minimization was accomplished using the Discover module of the Biosym molecular modeling package and the CVFF force field, modified to accommodate the cytochrome *c* heme group (D. Haney and J. S. Fetrow, unpublished). The molecule was minimized *in vacuo* with no charges for 50 iterations of steepest descents minimization with all atoms constrained, except the last three residues of the C-terminal helix. This was followed by 1000 iterations of minimization using a conjugate gradients algorithm, with all but the final three residues of the protein very weakly constrained. As a control, this strategy was applied to the iso-1-cyt *c* crystal structure and was found to be sufficient to remove all steric overlaps without significantly perturbing the molecule. When this strategy was applied to the spin-labeled protein, the final energy was within the range of that of the wild type protein.

RESULTS

Equilibrium Characterization of C102-SL. The EPR spectra of C102-SL under folded and under chemically and thermally denatured conditions are compared. Figure 2A shows the absorption derivative ($d\chi''/dH$) EPR spectrum of C102-SL folded at 15 °C and pH 5. Since a derivative EPR signal may tend to enhance sharp features, whereas a direct absorption presentation renders broad features more obvious, Figure 2B gives the direct absorption EPR signal (χ''), obtained as a first integral of Figure 2A. There was no evidence of a broad, immobilized signal in Figure 2B as might appear from aggregated material. The spectrum of C102-SL denatured by 2 M GdnHCl at 15 °C and the spectrum of C102-SL denatured by heat at 75 °C are shown in parts C and D of Figure 2, respectively; the narrowing and sharpening of features and the increased ratio of outlying ($M = \pm 1$) to central ($M = 0$) features imply more rapid probe tumbling when the protein is denatured. Figure 2E compares the $d\chi''/dH$ absorption derivative spectra of the same concentration of folded and GdnHCl-unfolded protein at the same conditions (2 °C and pH 5.0) used for the stopped-flow experiments. The dotted lines in Figure 2 are from simulations after Schneider and Freed (1989). As an empirical measure for following equilibrium thermal denaturation, the ratio of $H(-1)/H(0)$ EPR peak heights is presented in Figure 3A and is compared to changes in the following other measures of denaturation: far-UV CD at 222 nm, UV at 280 nm, and UV−Vis at 399 nm. Figure 3B shows that there was a change in the nature of the probe motion upon thermal folding as indicated by the $|C/B|$ ratio increasing significantly above unity at lower temperatures. In Figure 3C, the increasing $H(-1)/H(0)$ ratio provides a measure of denaturation by GdnHCl. In summary, these data showed that the EPR signal exhibits distinct signatures for native and denatured protein and that the EPR line shape can be used to monitor a cooperative folding transition.

The existence of a low-spin ferric heme iron near the spin probe may lead to line broadening of a spin-label signal which at cryogenic temperatures could provide information on iron−nitroxide distances [after Mascarenhas et al. (1983)]. Because of the low-spin ferric heme, the nitroxide spin (here on the spin-label) could experience an internal electron spin−spin interaction field, called $\pm 1/2\Delta H_{ss}$, which will be quantized either along or against the applied magnetic field. The overall change in the nitroxide EPR line shape (either splitting, if ΔH_{ss} is large enough, or broadening) can be

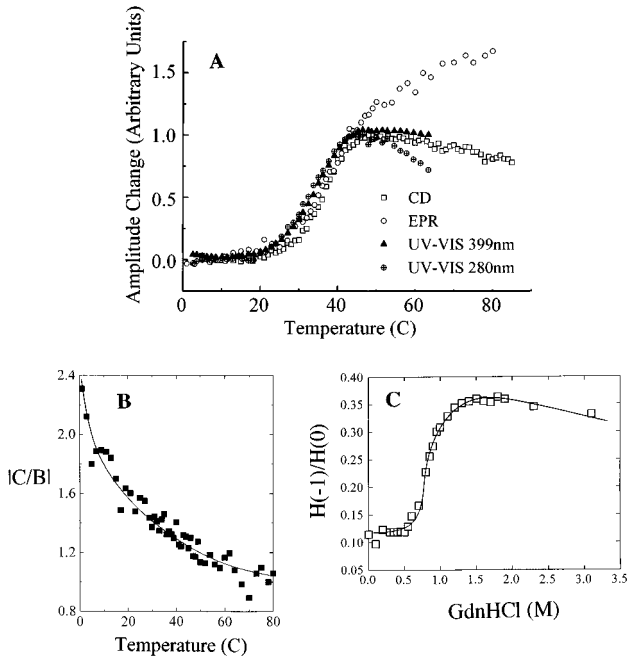

FIGURE 3: (A) Thermal melting of C102-SL as monitored by CD at 222 nm (open squares), UV−Vis at 399 nm (filled triangles), UV−Vis at 280 nm (crossed circles), and EPR (open circles) from the ratio of $H(-1)/H(0)$. A change of 1.0 unit on the vertical axis $= 4 \times 10^{-3}$ mean residue ellipticity CD units at 222 nm, 0.075 absorbance unit at 399 nm, 0.02 absorbance unit at 280 nm, and 0.4 unit in $H(-1)/H(0)$. This work was done at pH 5.0 in 0.1 M sodium acetate buffer. (B) The $|C/B|$ ratio determined via eqs 2 and 3 as a function of temperature. (C) GdnHCl-induced denaturation of C102-SL shown by the ratio of $H(-1)/H(0)$.

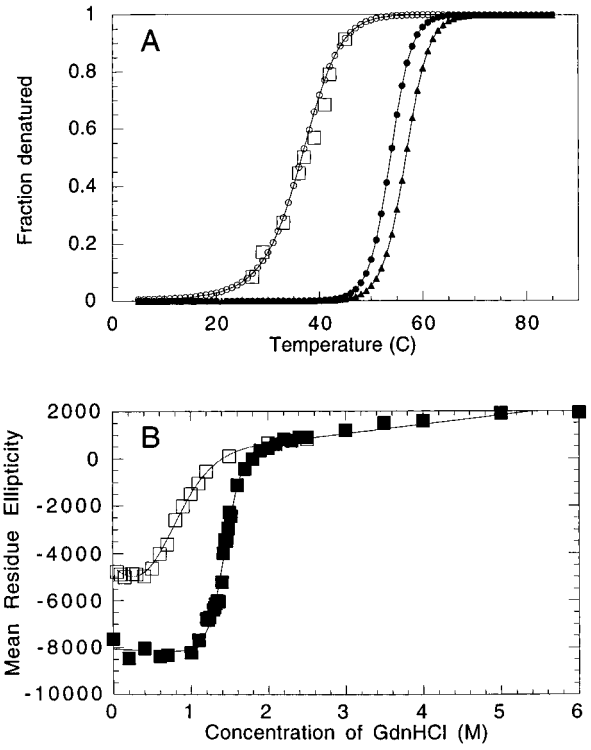

FIGURE 4: (A) Temperature dependence of the fraction of denatured protein: for C102T (filled triangles), for C102 (filled circles), and for C102-SL (open circles), all as monitored by CD, and for C102-SL as monitored by EPR (open squares). As outlined in Materials and Methods, the fraction melted was determined from CD measurements such as those shown in Figure 3A after the method of Cohen and Pielak (1994), while for EPR data, the fraction melted was determined from least-squares fitting of partially melted EPR spectra. (B) GdnHCl denaturation for C102 and C102-SL (filled squares) and C102-SL (open squares) showing equilibrium unfolding behavior of the proteins as monitored by far-UV CD spectroscopy at 5 °C and pH 5.0. The curves are a nonlinear least-squares fit of eq 4 of Santoro and Bolen (1988) to the data.

estimated from the EPR line broadening at cryogenic temperatures.[3] On comparison of uncomplexed MTSSL to R1 attached to C102-SL at 10 K, we determined that the line widths of all attached probe features increased by <1 G (as shown in Figure S-1 of the Supporting Information).

CD and UV−visible spectroscopy were used to compare spectra and equilibrium denaturation characteristics of C102-SL, C102, and C102T. The far-UV CD of C102 and the C102T variants exhibited similar helical content, while C102-SL exhibited a native-like but decreased helical signature (Figure S-2A of the Supporting Information). Small changes in the near-UV CD spectra were seen after the addition of the spin label to C102 (Figure S-2B of the Supporting Information). Visible heme spectra for C102 and C102T can be overlaid with those for C102-SL (Figure S-3 of the Supporting Information), implying that the heme environments were similar.

The thermal and chemical denaturation curves in panels A and B of Figure 4 clearly show that the spin-labeled protein is a protein that folds cooperatively. Coincidence of fractions denatured, as inferred from both CD and EPR in Figure 4A, made it clear that EPR of the spin-label attached to the C terminus of C102-SL and far-UV CD of the overall secondary helical content of C102-SL were measuring the same equilibrium thermodynamic folding process. However, the C102-SL thermal denaturation plot of Figure 4A displayed thermodynamic differences from the plot of the unlabeled C102T and C102 proteins. Table 2 summarizes the thermodynamic parameters determined by the methods of Cohen and Pielak (1994). For C102-SL, the melting temperature T_m decreased by 18 °C, the enthalpy of folding decreased by about 50 kcal mol^{-1}, and the free energy of folding at 300 K ($\Delta G_{300\ K}$) decreased by approximately 5 kcal mol^{-1}. The GdnHCl denaturation plot of Figure 4B likewise showed a difference between the chemical melting behavior of C102 and C102-SL, most obviously the fact that the C_m diminished by 0.6 M from 1.4 to 0.8 M. Values of m and ΔG_{H_2O} at 5 °C are given in Table 2, and the resultant fits are superimposed in Figure 4B. Compared to those for C102, the values of m and ΔG_{H_2O} at 5 °C diminished for C102-SL from 5.4 to 3.8 kcal mol^{-1} M^{-1} and from 7.8 to 3.1 kcal/mol, respectively. The consistency of ΔG_{H_2O} at 5 °C as calculated from thermal denaturation information (Figure 4A) and from GdnHCl melting information (Figure 4B) is a sign that the same melting process was being measured by both types of denaturation.

[3] When there is a Gaussian line EPR shape with a natural width ΔH_i (ΔH_i = width between derivative extrema) and a spin−spin interaction whose strength in magnetic field units is $\pm 1/2\Delta H_{ss}$, the Gaussian line width is increased by this additional random field to $\Delta H = (\Delta H_i^2 + \Delta H_{ss}^2)^{1/2}$. The central $M = 0$ EPR feature has an intrinsic Gaussian line width due to unresolved proton hyperfine structure in the absence of such an additional spin−spin interaction. When the line width increased by 1 G from $\Delta H_i = 10$ G to $\Delta H = 11$ G, then $\Delta H_{ss} \approx 5$ G. The dipolar interaction, ΔH_{ss}, is given by $\Delta H_{ss} = g_e\beta_e/r^3$ for two interacting $g_e = 2$ electrons and is on the order of 5 G when the interelectron distance $r \sim 15$ Å. We resolved such a dipolar interaction to estimate the distance between the heme irons of cytochrome *a* and a_3 in cytochrome *c* oxidase (Mascarenhas et al., 1983).

Table 1: Correlation Times from Line Shape Analyses

		correlation times from empirical line shape analysis						from simulation[d]	
sample	conditions	B^a (G)	C^a (G)	$\tau_{iso}(B)^b$ (ns)	$\tau_{iso}(C)^b$ (ns)	$\tau_\perp{}^c$ (ns)	$\tau_\parallel{}^c$ (ns)	$\tau_\perp$ (ns)	$\tau_\parallel$ (ns)
C102-SL	15 °C	-1.23 ± 0.13	1.87 ± 0.13	1.54 ± 0.18	1.91 ± 0.14	3.5 ± 1.0	1.1 ± 0.3	2.8	0.7
C102-SL	2 M GdnHCl and 15 °C	-0.35 ± 0.03	0.44 ± 0.03	0.44 ± 0.02	0.45 ± 0.02	0.45 ± 0.2	0.45 ± 0.2	0.35[e]	0.35[e]
C102-SL	70 °C	-0.084 ± 0.007	0.106 ± 0.009	0.11 ± 0.02	0.11 ± 0.009	0.12 ± 0.06	0.10 ± 0.04	0.1[e]	0.1[e]
H39C-SL	15 °C	-1.58 ± 0.31	2.88 ± 0.32	1.98 ± 0.50	2.94 ± 0.32	7.1 ± 2.5	1.1 ± 0.5	4.5	1.0

[a] Corrected for inhomogeneous broadening after Bales (1989, p 111). Uncertainties in *B* and *C* estimated from propagation of errors in $H(0)$, $H(-1)$, and $H(1)$ in eqs S-1 and S-2 of the Supporting Information after Bevington (1969). [b] Computed from the following formulas after Marsh (1989, pp 259−262) and Todd and Millhauser (1991, p 5517): $\tau_B = (H)^{-1}\,(4.26 \times 10^6)B$ (Gauss) and $\tau_C = (1.02 \times 10^{-6})C$ (Gauss). Uncertainties estimated from propagation of errors in $H(0)$, $H(-1)$, and $H(1)$ after Bevington (1969). [c] Computed after Marsh (1989, pp 260 and 261) with the nitroxide *y* axis as the rapid axial diffusion direction. The simulation on folded C102-SL was consistent with the axis for rapid anisotropic diffusion lying $\leq 30°$ off the *y* magnetic axis of the probe. [d] Obtained from the simulations with the program of Schneider and Freed (1989) to data of Figures 2A−C. [e] Obtained from simulations with isotropic correlation times.

Table 2: Thermodynamic Folding Parameters

(A) From Thermal Denaturation[a]			
protein variant	T_m (K)	ΔH (kcal mol^{-1})	$\Delta H_{300\,K}$ (kcal mol^{-1})
C102T[b]	54.7 ± 1.5	81.3 ± 12.1	6.4 ± 0.4
C102[b]	54.3 ± 0.6	91.8 ± 17.6	6.5 ± 0.2
C102-SL[c]	35.7 ± 2.0	42.8 ± 8	1.4 ± 0.2

(B) From GdnHCl Denaturation[d]				
protein variant	C_m (M)	ΔG_{H_2O} (kcal mol^{-1})	m (kcal M^{-1} mol^{-1})	ΔG (kcal mol^{-1})[f]
C102	1.4 ± 0.13	7.8 ± 0.5	5.4 ± 0.3	10.0
C102-SL[e]	0.81 ± 0.12	3.1 ± 0.3	3.8 ± 0.4	2.8

[a] Performed in 0.1 M sodium acetate buffer at pH 5. Equilibrium transition curves were calculated by nonlinear least-squares analysis described in Materials and Methods. Explicit values of thermodynamic parameters and melting points as experimentally generated by CD at 222, 281.5, and 287.5 nm, UV−Vis at 280, 287, 360, and 399 nm, and EPR are given in Table 1S of the Supporting Information. [b] Obtained from average numbers from CD and UV−Vis analyses. [c] Obtained from average numbers from CD, EPR, and UV−Vis analyses. [d] Obtained at 5 °C with cyt *c* solutions containing 0.1 M sodium acetate at pH 5.0 and from CD analysis after Santoro and Bolen (1988). [e] From the EPR plot of $H(0)/H(1)$ of C102-SL (Figure 3C), we determined that $C_m = 1.0 \pm 0.05$ M, $\Delta G_{H_2O} = 2.9 \pm 0.1$ kcal mol^{-1}, and $m = 3.0 \pm 0.1$ kcal M^{-1} mol^{-1}. [f] Evaluated from parameters generated from the thermal denaturation experiments, independent of these GdnHCl denaturation experiments.

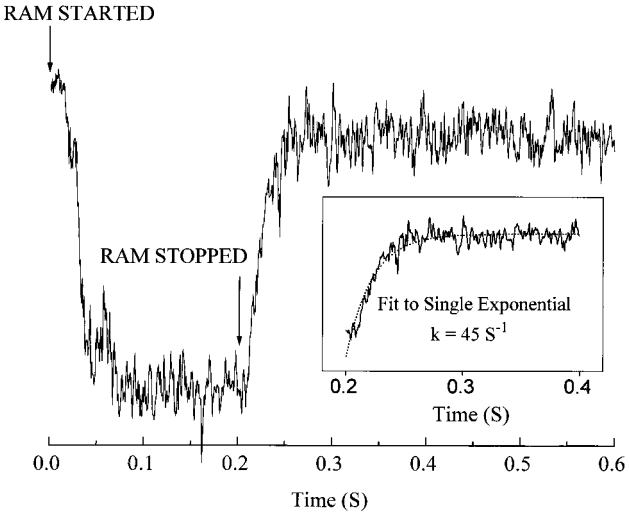

FIGURE 5: Kinetic unfolding transient EPR signal following 1/1 mixing of 80 μM C102-SL in 0.1 M phosphate buffer with 4 M GdnHCl at pH 6.5 to give a final concentration of 40 μM C102-SL and 2 M GdnHCl. The central $H(0)$ EPR feature was monitored with a field modulation of 1 G ptp, with an experimental EPR time constant of 1 ms. The vertical axis is the EPR signal, and its height represents ~ 47% of the static difference between the completely folded signal in acetate buffer and the unfolded signal in 2 M GdnHCl. Arrows indicate where flow stopped and started. The data presented are the result of two summed transients. The inset shows the fit of the kinetic transient to a single exponential with an unfolding rate constant *k* of 45 s^{-1}.

Stopped-Flow Kinetic Study of C102-SL. Figure 5 shows the kinetic unfolding transient, induced by a GdnHCl concentration (after mixing) of 2 M at pH 6.5 and 2 °C. The inset shows the fit to a single exponential with a time constant of 22 ms (at an unfolding rate *k* of 45 s^{-1}). The concentration of C102-SL after 1/1 mixing of concentrated GdnHCl with folded protein in dilute phosphate buffer was 40 μM, and the kinetic transient of Figure 5, which was observed at the central derivative EPR maximum, is the summed result of two shots which consumed a total of 130 μL of 80 μM C102-SL.

The kinetic behavior of separate GdnHCl-induced unfolding experiments at GdnHCl concentrations (after mixing) that varied from 0.9 to 2.0 M is compared in Figure S-5 of the Supporting Information. Such unfolding kinetics were monoexponential, and there was a marked GdnHCl concentration dependence on the rates which at pH 6.5 increased from 2 to 45 s^{-1} as the GdnHCl concentration increased from 0.9 to 2.0 M. Increasing the flow rate from 660 to 1320 μL/s increased the observable unfolding. Spectra C and C′ of Figure S-5 of the Supporting Information provide evidence that unresolved unfolding within the mixing time of the apparatus diminished by about 22% upon increasing the flow rate from 660 to 1320 μL/s. Optically detected stopped flow of C102-SL (Figure S-5E) also showed an unfolding rate comparable to that observed by EPR when the two traces were obtained under the same conditions (pH 5.0 and 0.9 M GdnHCl). For a given GdnHCl concentration, unfolding occurred generally at a faster rate at pH 5.0 than at pH 6.5.

Next, the kinetically more complex refolding process was followed. Much of the work was done under conditions where the unfolded protein was mixed with dilute buffer to a final state ([GdnHCl] = 0.9 M, $T = 2$ °C) at which the protein would become about half-folded at equilibrium. This was a state where a wide range of kinetic processes and time regimes were measurable by stopped-flow EPR and UV−Vis and where folding as well as unfolding could be measured under the same final denaturant conditions. Stopped-flow EPR carried out at pH 6.5 (Figure 6A and Table 3) indicated multiphasic behavior where ~44% of the recovery was at a faster rate of 12 s^{-1} (80 ms), 31% of the recovery was at an intermediate rate of $k = 1.2$ s^{-1} (800 ms), and

Table 3: Refolding Rates and Amplitudes for C102-SL

conditions	k_o (s^{-1})[c]	A_o[d] (%)	k_1 (s^{-1})	A_1 (%)	k_2 (s^{-1})	A_2 (%)
(A) Data from Stopped-Flow EPR[a]						
pH 6.5 (2 °C)[b]	>125	25 ± 3	11.9 ± 2.3	44 ± 4	1.2 ± 0.2	31 ± 3
pH 5.0 (2 °C)[b]	>125	35 ± 6	6.2 ± 0.7	65 ± 5	–	–
pH 5.0 (2 °C) and 0.6 M GdnHCl	>125	45 ± 3	9.5 ± 0.8	55 ± 3	–	–
pH 5.0 (10 °C)[b]	>125	52 ± 5	17.2 ± 2.2	48 ± 4	–	–
pH 5.0 (18 °C)[b]	>125	77 ± 7	41.7 ± 3.4	23 ± 6	–	–

conditions	k_1 (s^{-1})	A_1[e] (%)	k_2 (s^{-1})	A_2 (%)	k_3 (s^{-1})	A_3 (%)
(B) Data from Stopped-Flow UV−Vis						
pH 6.5 (2 °C)[f]	–	–	1.8 ± 0.1	75 ± 9	0.2 ± 0.03	25 ± 5
pH 5.0 (2 °C)[g]	63 ± 14	100	–	–	–	–

[a] Amplitude changes based on CW EPR spectra taken before and after folding from the same concentration of C102-SL. [b] Final GdnHCl concentration is 0.9 M GdnHCl after 1/1 mixing of C102-SL with buffer. [c] k_0 for EPR is based on a dead time of 8 ms (>125 s^{-1}). [d] Errors in A_1, k_1, A_2, k_2, A_3, and k_3 from standard deviation in nonlinear least-squares analysis of kinetic transients. Error in A_o of EPR kinetics estimated from propagation of noise errors in the height of overall transient signal and noise errors in the initial unfolded and the final refolded equilibrium EPR signals. [e] Amplitude change during mixing (A_o) not measured with single-beam Aminco-Murrow stopped-flow system. Amplitude estimates based on change observed after flow stopped. [f] Measured at 407 nm. [g] Measured at 410 nm.

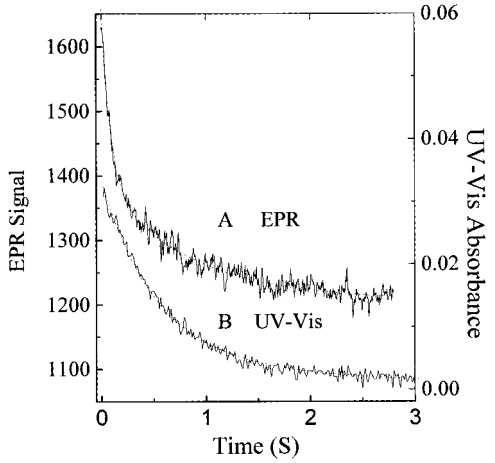

FIGURE 6: This figure provides a comparison of the EPR and UV−Vis stopped-flow kinetics of protein refolding where initially unfolded protein in 1.8 M GdnHCl at pH 6.5 was mixed in a 1/1 fashion with 0.1 M phosphate buffer at pH 6.5 and 2 °C. (A) The EPR trace exhibited biphasic behavior with rates of 12 and 1.2 s^{-1}. (B) The UV−Vis kinetic trace obtained at 407 nm exhibited a slower biphasic behavior with rates of 1.8 and 0.2 s^{-1}.

25% of the signal was recovered during the mixing time. UV−Vis stopped flow, as reported by the heme at 407 nm in Figure 6B, also indicated biphasic behavior having an intermediate rate of 1.8 s^{-1} (550 ms) that accounted for 75% of the recovery; furthermore, UV−Vis showed an even slower rate of 0.2 s^{-1} (5 s). (As discussed in Materials and Methods, we did not attempt to estimate the percent change in UV−Vis signal during the dead time.) The expected multiphasic behavior thought to be due to heme misligation during folding (Sosnick et al., 1994) did occur and was obvious not only because of the large intermediate phase in heme absorbance kinetics but also because of an intermediate time phase in the spin-label kinetic recovery.

At pH 5.0, the complication of heme misligation during refolding is less apt to occur because of protonation of relevant histidines (Sosnick et al., 1994; Elöve et al., 1994), and the kinetics we observed at this pH were monophasic. In Figure 7 A, we show the spin-label's time-dependent refolding at 2 °C, where the concentration of GdnHCl after mixing was 0.9 M. The rate for refolding was $k = 6.2$ s^{-1}; 65% of the refolding was observed with this rate, while 35% of the refolding occurred within the mixing time (<∼8 ms).

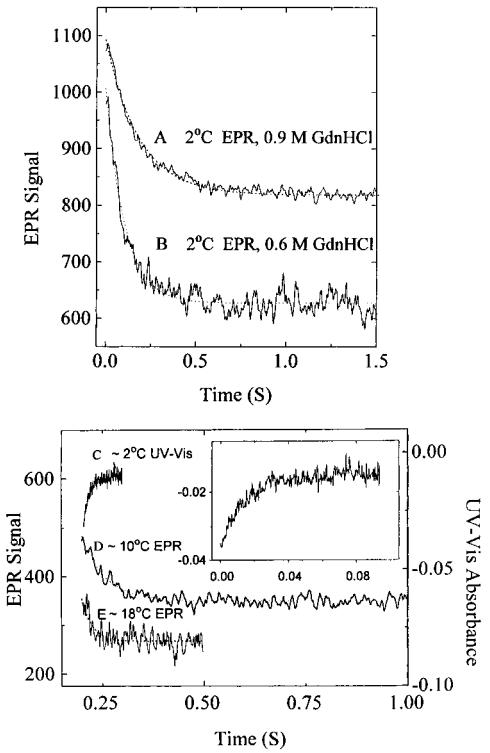

FIGURE 7: Refolding behavior at pH 5.0 where single-exponential, monophasic behavior was observed. For the refolding experiments of traces A and C−E, initially unfolded protein in pH 5.0, 1.8 M GdnHCl was mixed in a 1/1 fashion with 0.1 M acetate buffer at pH 5.0. Trace A exhibits the EPR refolding kinetics at 2 °C which occurred with a rate of 6.2 s^{-1}. For trace B, the refolding kinetics occurred at a lower GdnHCl concentration of 0.6 M obtained by mixing denatured protein in 1.8 M GdnHCl at pH 5.0 in a 1/2 fashion with 0.1 M acetate buffer at pH 5.0; the rate of refolding was 9.5 s^{-1}. Trace C and the inset exhibit the UV−Vis refolding kinetics observed at 410 nm and at 2 °C which occurred with a rate of 62 s^{-1}. Traces D and E show the refolding EPR refolding kinetics at 10 and 18 °C, for which the respective rates were 17 and 42 s^{-1}.

A GdnHCl concentration of 0.6 M is in a concentration regime where refolding predominates more than at 0.9 M for C102-SL. The apparent equilibrium constant is ∼5 in favor of the folded form when the GdnHCl concentration is 0.6 M.[6] Therefore, as shown in Figure 7B, refolding at 0.6 M GdnHCl versus 0.9 M GdnHCl increased the refolding rate by 50% to 9.5 s^{-1}. EPR kinetic traces D and

E of Figure 7 indicate that the rate for refolding increased markedly with temperature; the rate was 3-fold faster (rate of 17 s^{-1}) at 10 (±2) °C and 6-fold faster (rate of 42 s^{-1}) at 18 (±1) °C. Kinetic recovery during the mixing time significantly increased at these higher temperatures as indicated in Table 3. In contrast to its slow, multiphasic recovery at pH 6.5, the UV−Vis stopped-flow kinetics as reported by the heme absorbance showed (Figure 7C and inset) a very fast recovery with a rate of 50 s^{-1} and no evidence of any slow or intermediate step. The maximum UV−Vis change monitoring heme ligation for pH 5 refolding occurred at a wavelength (410 nm) slightly different from that for pH 6.5, and the sense of this optical signal change shown in Figure 7C was the opposite of that at pH 6.5.

DISCUSSION

Overview. Stopped flow has been available since the 1950s for elucidation of chemical kinetics, and spin labeling has been used since the 1960s for elucidation of nanosecond molecular motion. The 20 ms stopped-flow EPR time scale is unprecedented for any spin-labeled protein system (Figures 5, 7, S-4, and S-5). Stopped-flow EPR gives a new temporal component to probing nanosecond macromolecular motions as the character of such motions evolves from milliseconds to seconds. Such motional evolution might occur, for example, in conformational changes of spin-labeled proteins or in time-resolved immobilization of spin-labeled substrates. The amount of protein used for the EPR transients that provided Figures 5−7 was <150 μL of an 80 μM solution; stopped-flow EPR provides a new method for the kinetic study of precious mutant protein. The amount of protein needed for stopped-flow EPR is overwhelmingly less than that used for NMR-detected pulse labeling which requires multiple mixings, quenchings, and reconcentration (Roder et al., 1988). Spin labeling yields dynamic information on the specific environments of probe attachment (e.g., the C-terminal helix in the work reported here) as a complement to fluorescence which provides a general measure of heme−tryptophan separation (Tsong, 1976) or as a complement to CD which measures the general state of secondary structure. Stopped-flow CD appears to require >40 shots per experiment for adequate signal to noise (Elöve et al., 1992). Our data are the result of two shots per experiment.

Equilibrium Characterization of C102-SL. The focus of the work reported here was to take a major methodological step forward in the union of stopped flow and spin labeling. However, it was important to characterize C102-SL, yeast iso-1-cyt *c* labeled at the available naturally occurring cysteine, because C102-SL is the starting point for the kinetic study and for the design of future systematic experiments on site-directed cysteine mutants. To provide the proper underpinnings we (1) characterized the motion of the C102-SL nitroxide probe under folded and unfolded conditions, (2) estimated the location of the probe, (3) delineated spectroscopically and thermodynamically the perturbation caused by the probe, and (4) used molecular mechanics to simulate pertrubation of the protein structure by the probe.

Although Cys^{102} is the penultimate C-terminal amino acid, its cysteine sulfur is 99.4% buried within the protein interior 11 Å from the heme (Figure 1). The temperature factors, for both the side chain and backbone atoms of Cys^{102}, are about the average of those for the entire iso-1-cyt *c* molecule (Louie & Brayer, 1990). The initial site of probe attachment, the C terminus of the cytochrome C-terminal helix, therefore is not a frayed area of high mobility in the native protein. Not unexpectedly, the comparison of folded and unfolded C102-SL (Figure 2) showed that the probe tumbling slowed when the protein is folded. Correlation times determined from peak heights (see eqs S-1−S-4 in the Supporting Information) increased to greater than 1 ns in the folded protein. When the protein folded, the motion did not just slow. The explicit correlation times changed from those reporting rapid isotropic tumbling in denatured protein[2] to those reporting slower anisotropic tumbling in the folded protein (Table 1). Correlation times longer than ∼1−2 ns are at the limit of the simple, semiempirical, fast-tumbling treatment that explains B and C, and so simulations (Schneider & Freed, 1989), not limited by such a simple treatment, were overlaid as dotted lines with the experimental spectra of Figure 2 to verify the empirical estimates on correlation times and anisotropy of tumbling. The nitroxide probe of folded C102-SL is anisotropically tumbling about a "fast axis" with a correlation time $\tau_{||}$ of ∼0.7 ns, and perpendicular to this fast axis, there is slower tumbling, $\tau_{\perp}$ of ∼ 3 ns, compatible with tumbling of the protein as a whole. Describing the motion with an anisotropic diffusion tensor with orthogonal || and ⊥ axes is only an approximation since the bonds which link the nitroxide to the backbone are not orthogonal. It has been suggested that the true anisotropic motion is a rapid, restricted rotation about the $C_{\delta}-C_{\epsilon}$ and $S-C_{\delta}$ bonds that serves to move the probe *z* axis (p_{π} orbital) within a finite cone (Mchaourab et al., 1996).

From EPR of spin-labeled protein near room temperature, we estimated the tumbling motion of the spin-label; from cryogenic EPR, we estimated the location of the nitroxide spin with respect to the heme iron. An increase of <1 G in a 10 G cryogenic line width (Figure S-1) can be accounted for by an internal dipolar field ΔH_{ss} of <5 G, and the distance between the nitroxide and the heme iron would thereby turn out to be greater than 15 Å.[3] Such a weak dipolar interaction

[4] The contribution to the dynamically broadened ambient temperature spin probe line width, δH (in Gauss), from distance-dependent, dipolar interaction is as follows. $\delta H = (5 \times 10^{15})\tau_e/R^6$, where R (in angstrom) is the iron to nitroxide distance and τ_e is the ferric heme electron spin relaxation time (Fielding et al., 1986). Under ambient conditions, τ_e has been estimated at 2×10^{-12} s for the heme iron of low-spin ferric cytochrome *c* (Keller & Wüthrich, 1981), and the UV−Vis spectrum of our cytochrome *c* indicates that the heme is low-spin ferric. The expected broadening, δH, of the ambient temperature line shape would be expected to be <<<1 G. The inference is that the ambient temperature EPR line shape of the probe attached to cytochrome *c* reflects probe/protein tumbling, *not* spin−spin interaction between probe and low-spin ferric iron.

[5] For C102-SL, the EPR methods of Lindgren et al. (1995) were used to probe for multiple inflection points which might occur in thermal or chemical melting curves if there were multiple, significantly populated equilibrium states beyond the folded and the unfolded, denatured states. No additional inflection point beyond the expected one at T_m or C_m was found.

[6] If the folding/unfolding equilibrium were a simple two-state equilibrium between unfolded (U) and native (N) species where U ⇔ N, then the equilibrium constant would be $K_{eq} = k_f/k_u$. The apparent rate constant, k_{app}, for the approach to equilibrium, either from initial strong denaturing conditions or from initial fully native conditions, should be $k_{app} = k_f + k_u$. There was a rationale for doing refolding experiments at the final condition of 0.6 M GdnHCl, where the equilibrium is toward refolding. If kinetic measurements were to yield an apparent rate constant with contributions from unfolding and refolding, the contribution of the refolding rate to the apparent first-order rate would be much the larger when the equilibrium is strongly toward refolding.

will have no effect on the spin probe line widths at room temperature.[4] The implication of the cryogenic EPR result is that the nitroxide ring itself points generally away from the heme iron so that its dipolar interaction with the heme iron is negligible and the probe−iron distance is greater than 15 Å. The marked difference in mobility between folded C102-SL and unfolded C102-SL implies that the R1 probe which has found its way out to the protein periphery is constrained out through the $C_\delta-C_\epsilon$ and $S-C_\delta$ bonds as it was in T4 lysozyme (Mchaourab et al., 1996).

Our thermodynamic measurements and far- UV CD measurements indicate that the nitroxide ring and its tether perturb helical packing interactions and decrease the ΔH of folding and the *m* parameter, but not in such a way that the protein fails to fold. The value of *m* is thought to be proportional to the difference in accessible surface area between the unfolded and native states (Schellman, 1978); thus, a decrease in *m* would require an increase in the solvent accessible area of the folded protein or a decrease in the solvent accessible area of the denatured protein. An explanation for our ∼30% decrease of *m* parameter in the presence of probe is that the probe increases the solvent accessible area of the folded protein. A significant decrease in ΔH and *m* has been associated in mutant forms of staphylococcal nuclease with an equilibrium folding intermediate and with loss of folding cooperativity between two domains of that protein (Carra et al., 1994; Carra & Privalov, 1995). We found no spectroscopic evidence in C102-SL for such an intermediate,[5] and we would have expected multiple-exponential unfolding behavior (not seen) if there were more than one equilibrium folding intermediate. In potentially relevant work to MTSSL labeling at a buried cysteine, Wynn and Richards (1993) modified a buried cysteine of thioredoxin with a series of straight chain aliphatic thiosulfonates, and diminished *m* parameters were found. However, the correlation of aliphatic chain length to the *m* parameter was not straightforward since their shortest and intuitively less perturbing attachment ($S-CH_3$) caused an ∼40% decrease in *m*, while their longest and intuitively more perturbing attachments (*n*-butyl and *n*-pentyl) caused ∼16% decreases in *m* (Wynn & Richards, 1993). The probe-induced decreases in free energy, enthalpy, and melting temperature which we observed fell within the range of values found for substitutions by single native amino acids at buried sites in T4 lysozyme (e.g., that of $Leu^{99} \rightarrow$ Ala which caused little physical distortion; Eriksson et al., 1993) and at buried sites in iso-1-cyt *c* [e.g., those of $Phe^{10} \rightarrow$ Met, $Lys^{94} \rightarrow$ Ala, and $Tyr^{97} \rightarrow$ Ala where all of these are in N or C helices (Pielak et al., 1995)].

Model building provided a rationale as to how the nitroxide probe may be situated at the protein surface, how the tether of the probe may be constrained in finding its way from the cysteine sulfur, and how the probe perturbs protein structure. The bound R1 probe has small size and conformational flexibility so that simple rotations about the $C_\alpha-C_\beta$ and $C_\beta-S_\gamma$ bonds (side chain dihedral angles χ_1 and χ_2, respectively, as shown in the structure in the introductory section) easily moved the nitroxide ring to the protein surface. The resulting structure was then used as the basis for the energy minimization. Upon completion of the minimization, the probe was still located at the protein surface, 20 Å from the heme iron. Figure 1B shows the orientation of the R1 spin-label with respect to the C-terminal helix. The methylene and sulfhydryl groups connecting the nitroxide ring to the backbone were largely buried within the protein, and motion about their bonds was constrained; however, a simple conformational search showed that rotation about the terminal side chain dihedral angle in R1 (which is rotation about the $C_\delta-C_\epsilon$ bond) was relatively unconstrained. As Mchaourab et al. (1996) determined, it is this remaining motion about the $C_\delta-C_\epsilon$ bond that is detected by the spin-label in the folded protein. In the modeled and minimized C102-SL structure, there was actually about 3% less solvent accessible area of both hydrophobic and hydrophilic atoms in C102-SL than in native C102. When R1 was incorporated, there was a general increase in $(C{=}O)_i$ to $(NH)_{i+4}$ hydrogen bond lengths within the C-terminal α-helix, consistent with unwinding and possible fraying of the helix. The last two hydrogen bond lengths ($O_{97}\cdots N_{101}$ and $O_{98}\cdots N_{102}$) increased by ∼0.5 Å to well beyond the proper length of an α-helical hydrogen bond. Such a perturbation to the helix may account for the reduced CD helical signature and the diminished ΔH of folding.

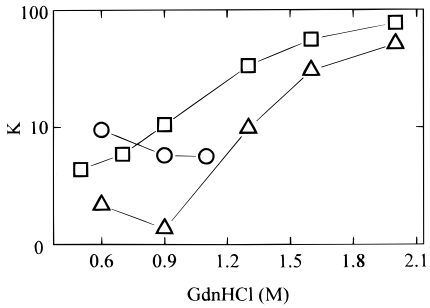

FIGURE 8: Logarithmic plot of folding and unfolding rates as a function of GdnHCl concentration: unfolding rate (open triangles) at pH 6.5, unfolding rate (open squares) at pH 5.0, and refolding rate (open circles) at pH 5.0.

Unfolding Kinetics of C102-SL. Our GdnHCl unfolding monitored by stopped-flow EPR and UV−Vis of C102-SL is consistent with unfolding as a single global event reported similarly by all types of spectroscopy, and it showed a GdnHCl concentration dependence qualitatively similar to that of the unfolding monitored by fluorescence of horse cyt *c* and of its C-terminal Lys^{94} mutants (Colón et al., 1996). Above the midpoint (C_m = 0.8 M) of the folding transition for C102-SL, the unfolding rate markedly increased but showed evidence of leveling off at high concentrations. The rate of GdnHCl-induced unfolding reported here for C102-SL had already reached ∼50 s^{-1} when the GdnHCl concentration was 2 M, whereas a GdnHCl concentration of 4 M was needed before wild type horse heart cyt *c* would unfold at a rate of ∼50 s^{-1} (Colón et al., 1996). This decrease in stability reflects primarily the intrinsic folding difference between horse cyt *c* (C_m = 2.7 M) and yeast iso-1-cyt *c* (C_m = 1.4 M) and secondarily the perturbation of the spin-label on C102-SL (C_m = 0.8 M). As discussed below, the rate of refolding for C102-SL is comparable to refolding rates for horse cyt *c* at similar GdnHCl concentrations and temperatures; it must be the much larger rate of unfolding at lower GdnHCl concentrations (<2.0 M) which accounts for the decreased native state equilibrium stability of C102-SL versus horse cyt *c*. The unfolding rates themselves are generally larger at pH 5.0 because the activation free energy to unfold may be smaller at pH 5.0 in the absence of GdnHCl. As shown in Figure 8, the rates of folding and

unfolding at pH 5.0 were comparable but not equal at GdnHCl concentrations below 0.9 M.[6]

Logarithmic denaturant plots of the unfolding rate constants versus GdnHCl concentrations are provided in Figure 8. These denaturant plots showed, especially at pH 6.5, a steep increase of the unfolding rate that started near the midpoint of the GdnHCl-induced unfolding transition (C_m ~ 0.8 M GdnHCl). This increase began to level off at ~50 s^{-1} toward higher GdnHCl concentrations of ≥2.0 M. Such behavior in the GdnHCl-unfolding rate, starting at the relevant C_m and increasing to about 50 s^{-1}, has been noted for other cytochromes [see Figure 5 of Colón et al. (1996)]. Colón et al. (1996) suggested that this steep refolding rate increase with GdnHCl concentrations implies that a major conformational unfolding transition that involves a large increase in denaturant accessible area exists. At pH 5, we found that on a log scale the refolding rate increase between 0.8 and 2.0 M GdnHCl was ~2-fold less steep than the corresponding increase at pH 6.5. It may follow that there is less increase in denaturant accessible area during unfolding at pH 5.0. The leveling at ~50 s^{-1}would imply the existence of a GdnHCl-independent process, such as Met^{80} dissociation form the heme, which precedes global GdnHCl-induced unfolding and which becomes rate-limiting at high GdnHCl concentrations (Colón et al., 1996).

Refolding Kinetics. The C102-SL spin-label kinetics of Figure 6A reported events faster than those associated with the >500 ms recovery from heme misligation. The largest amplitude fast event (44%) for C102-SL had a time constant of ~80 ms (11.9 s^{-1}), and there was an even faster phase (25%) that occurred within the dead time. As the systematic work of Mchaourab et al. (1996) on numerous R1-labeled sites of T4 lysozyme showed, the disulfide-attached spin probe motion reported the tertiary fold and, especially in cases where the probe was attached to an α-helix, backbone dynamics. Since R1 is attached to the C terminus of the C-terminal helix, our interpretation is that our kinetic experiments are sensing the change in probe dynamics which was concomitant with the formation of the C-terminal helix. Our interpretation is to assign the 80 ms phase to the N and C refolding step (but see the subsequent paragraph for detailed comparison with N and C refolding times from other techniques and with other cytochromes). The trace from UV−Vis stopped flow of C102-SL in Figure 6B and the data in Table 3 showed that the heme absorption reported 75% of its change at an intermediate rate (1.8 s^{-1}, 550 ms). The tryptophan fluorescence-monitored stopped-flow study of Zuniga and Nall (1986) on iso-1-cyt *c* modified at Cys^{102} by iodoacetamide also showed a preponderance of a form with a refolding time in an intermediate 1 s regime. The spin-label of C102-SL did not show the vast preponderance of intermediate time (>500 ms) recovery, but there was a component (31%) which reflected an intermediate time (800 ms) plausibly attributed to recovery from histidine misligation. The distant His^{26} and His^{33} have been proposed for misligation (Creighton, 1994); we note that in the crystal structure of iso-1-cytochrome *c* the terminal Glu^{103} (next to Cys^{102}) has a salt bridge to the imidazole of His^{33} (Louie & Brayer, 1990, p 548). If, in the course of folding at neutral pH, His^{33} or His^{26} is inappropriately liganding the heme, then that misligation would have to be undone and the proper His^{33}−Glu^{103} bridge with the C terminus established before proper folding of the C terminus could be reported by C102-SL.

At lower pH (5.0), the observable refolding recovery rate from C102-SL kinetics at pH 5.0, which we call our "fast" recovery rate, was 6.2 s^{-1} (160 ms) at 2 °C, and it increased 3-fold to 17 s^{-1} (60 ms) at 10 °C. There was an ~50% increase in our fast rate for refolding under the stronger refolding condition of 0.6 M GdnHCl (versus 0.9 M GdnHCl). The fast folding phase of horse heart cytochrome *c* reported by heme absorbance and fluorescence is in the 5−20 ms range and the time scale for N and C proton protection in the 15−30 ms range (Elöve et al., 1994), but this folding has been done at the higher temperature of 10 °C and at 0.7 M GdnHCl. There is reason for suspecting a species difference in refolding between horse and yeast iso-1-cyt *c* since, as observed by stopped-flow tryptophan fluorescence, the time for the fast refolding phase at the midpoint of the folding transition was 3-fold shorter (~15 ms) for horse cyt *c* than for yeast cytochrome *c* (~45 ms) (Brems & Stellwagen, 1983; Figure 5). For mutated horse cytochromes *c*, the rate of the fast folding process diminished 2−3-fold in the presence of perturbations to the N and C-terminal region caused by mutations at Lys^{94} in the C region (Colón et al., 1996), and by analogy, we must consider that the label-induced perturbation might slow N and C refolding. The somewhat slower EPR fast refolding times at pH 5 for C102-SL can be rationalized *vis-à-vis* the faster refolding times from the majority of studies on horse cyt *c* as being due to species difference, slightly different refolding conditions, and possibly probe perturbation.

At 2 °C and 0.9 M GdnHCl, the heme UV−Vis of C102-SL reported a fast 20 ms recovery; there was a substantial recovery phase for the spin-label signal during the EPR stopped-flow dead time. It can be asked whether these recoveries that are faster than 20 ms are due to C- and N-terminal helix pairing (Colón et al., 1996) or to molecular collapse (Sosnick et al., 1996). Such a molecular collapse is supposed to lead to significant burying of polar and nonpolar residues on the time scale of milliseconds and may or may not require the coformation of amino- and carboxyl-terminal helices (Sosnick et al., 1996). Since our label is attached to the C-terminal helix, since this particular spin-label has been shown in the hands of the Hubbell group (Mchaourab et al., 1996) to report the protein tertiary helical fold, and since we have presented evidence above that our observable kinetic phase in the 50−160 ms time regime is compatible with N and C refolding, the recoveries that are faster than 20 ms may be evidence for the molecular collapse described by Sosnick et al. (1996). A rapid phase reporting general molecular collapse should be similarly reported by probes at many different locations, whereas later folding events in helices and in loops should be specifically reported by probes placed in these regions. Experiments to test this hypothesis (see below) are underway.

Conclusions and Future Direction. Our kinetic measurements showed that stopped-flow EPR of a site-specifically attached spin-label can resolve with low reactant use kinetics of unfolding and refolding near the attachment site. The time resolution of our methodology is comparable with that reported from optical stopped-flow techniques. Having shown the utility of stopped-flow EPR for intimately probing the folding process, we believe a systematic experimental design is needed explicitly to elucidate the unfolding process

and to overcome limitations of the present cysteine[102]-labeled system. These limitations are the perturbation due to the probe as shown by diminished ΔH and T_m for thermal unfolding and diminished C_m and m parameters for GdnHCl denaturation; we also want to unequivocally delineate whether fast events are reporting molecular collapse or specific formation of folding units like N and C helices. The recent systematic site-directed spin labeling work of Mchaourab et al. (1996) on T4 lysozyme indicated that labels which are less perturbing and still immobilized can be incorporated into proteins by site-directed spin labeling at numerous external sites which have previously been mutated to cysteine. Such a systematic approach to labeling of yeast iso-1-cyt *c* may provide a method of probing with high sensitivity on small quantities of mutant protein the folding dynamics at numerous locations in different folding units (Bai et al., 1996) such as helices and loops. Promising preliminary equilibrium measurements have been recently done on small quantities of the mutant H39C, whose labeling site appears to fill the criteria of being immobilized yet less perturbing when labeled. H39C is a mutant which has had its natural Cys[102] converted to Thr and a new cysteine site created by the His[39] → Cys mutation. His[39] happens to be in a solvent-exposed loop. The EPR spectrum (parameters of it in Table 1) indicates that H39C-SL is more completely immobilized than C102-SL; yet T_m and C_m for H39C-SL are virtually identical to those of wild type C102.

ACKNOWLEDGMENT

The authors thank J. Spitzer for performing initial electrophoresis and HPLC characterization of labeled and unlabeled proteins, G. Pielak for supplying the yeast strain expressing the H39C protein, and R. Hansen, president of Update Instrument, Inc., for insights on stopped flow and mixing.

SUPPORTING INFORMATION AVAILABLE

Text to explain the following items: (1) empirical expressions to estimate rotational correlation times, (2) EPR line shape simulation via the software of Schneider and Freed (1989), and (3) how thermodynamic values were determined for spectroscopic data; Table 1S giving detailed thermal denaturation thermodynamic parameters for C102, C012T, and C102-SL as they were separately determined by CD, UV−Vis, and EPR; Table 2S providing GdnHCl denaturation parameters for C102 and C102-SL; and five figures comparing cryogenic EPR line widths from C102-SL and from MTSSL not attached to protein (Figure S-1), comparing CD spectra of C102, C102T, and C102-SL (Figure S-2A,B), comparing heme UV−Vis spectra from C102, C102T, and C102-SL (Figure S-3), comparing the amplitudes of stopped-flow EPR unfolding transients at two different flow speeds with the amplitudes of the appropriate folded and unfolded CW EPR spectra (Figure S-4), and comparing the kinetic behavior of separate GdnHCl-induced unfolding experiments at GdnHCl concentrations (after mixing) that varied from 0.9 to 2.0 M (9 pages). Ordering information is given on any current masthead page.

REFERENCES

Altenbach, C., Flitsch, S. L., Khorana, H. G., & Hubbell, W. L. (1989) *Biochemistry 28*, 7806−7812.

Altenbach, C., Marti, T., Khorana, H. G., & Hubbell, W. L. (1990) *Science 241*, 1088−1092.

Auld, D. S., & Pielak, G. J. (1991) *Biochemistry 30*, 8684- 8690.

Bai, Y., Sosnick, T. R., Mayne, L., & Englander, S. W. (1995) *Science 269*, 192−197.

Bales, B. L. (1989) in *Biological Magnetic Resonance* (Berliner, L. J., & Ruben, J., Eds.) Vol. 8, Chapter 2, pp 77−130, Plenum, New York.

Berghuis, A. M., & Brayer, G. D. (1992) *J. Mol. Biol. 223*, 959−976.

Berghuis, A. M., Guillemette, J. G., Smith, M., & Brayer, G. D. (1994) *J. Mol. Biol. 235*, 1326−1341.

Berliner, L. J., Ed. (1976) *Spin Labeling: Theory and Applications*, Academic Press, New York.

Betz, S. F., & Pielak, G. J. (1992) *Biochemistry 31*, 12337−12344.

Bevington, P. R. (1969) *Data Reduction and Error Analysis for the Physical Sciences*, Chapter 4, pp 56−65, McGraw-Hill, New York.

Brems, D. N., & Stellwagen, E. (1982) *J. Biol. Chem. 258*, 3655−3660.

Bushnell, G. W., Louie, G. V., & Brayer, G. D. (1990) *J. Mol. Biol. 214*, 585−595.

Carlsson, U., Aasa, R., Henderson, L. F., Jonsson, B.-H., & Lindskog, S. (1975) *Eur. J. Biochem. 52*, 25−36.

Carra, J. H., & Privalov, P. L. (1995) *Biochemistry 34*, 2034−2041.

Carra, J. H., Anderson, E., & Privalov, P. S. (1994) *Biochemistry 33*, 10842−10850.

Cohen, D. S., & Pielak, G. J. (1994) *Protein Sci. 3*, 1253−1260.

Colón, W., Elöve, G. A., Wakerm, L. P., Sherman, F., & Roder, H. (1996) *Biochemistry 35*, 5538−5549.

Cottrell, S. F., Rabinowitz, M., & Getz, G. S. (1975) *J. Biol. Chem. 250*, 4087−4094.

Creighton, T. E. (1994) *Nat. Struct. Biol. 1*, 135−138.

Cutler, R. L., Pielak, G. J., Mauk, A. G., & Smith, M. (1987) *Protein Eng. 1*, 95−99.

Elöve, G. A., Chaffotte, A. F., Roder, H., & Goldberg, M. E. (1992) *Biochemistry 31*, 6876−6883.

Elöve, G. A., Bhuyan, A. K., & Roder, H. (1994) *Biochemistry 33*, 6925−6935.

Elwell, M. L., & Schellman, J. A. (1977) *Biochim. Biophys. Acta 494*, 367−383.

Eriksson, A. E., Baase, W. A., & Matthews, B. W. (1993) *J. Mol. Biol. 229*, 747−769.

Farahbakash, Z. T., Hideg, K., & Hubbell, W. L. (1993) *Science 262*, 1416−1419.

Fetrow, J. S., Cardillo, T. S., & Sherman, F. (1989) *Proteins: Struct., Funct., Genet. 6*, 372−381.

Fetrow, J. S., Horner, S. R., Oehrl, W., Schaak, D. L., Burton, R. E., & Boose, T. L. (1997) *Protein Sci. 6*, 197−210.

Fielding, L., More, K. M., Eaton, G. R., & Eaton, S. S. (1986) *J. Am. Chem. Soc. 108*, 618−625.

Fredericks, Z. L., & Pielak, G. J. (1993) *Biochemistry 32*, 929−936.

Froncisz, W., & Hyde, J. S. (1982) *J. Magn. Reson. 47*, 515−521.

Hampsey, D. M., Das, G., & Sherman, F. (1986) *J. Biol. Chem. 261*, 3259−3271.

Hubbell, W. L., Froncisz, W., & Hyde, J. S. (1987) *Rev. Sci. Instrum. 58*, 1879−1886.

Jones, C. M., Henry, E. R., Hu, Y., Chan, C.-K., Luck, S. D., Bhuyan, A., Roder, H., Hofrichter, J., & Eaton, W. A. (1993) *Proc. Natl. Acad. Sci. U.S.A. 90*, 11860−11864.

Keller, R. M., & Wüthrich, K. (1981) in *Biological Magnetic Resonance* (Berliner, L. J., & Ruben, J., Eds.) Vol. 3, Chapter 1, Table I, Plenum, New York.

Lindgren, M., Svensson, M., Freskgård, P.-O., Carlsson, U., Jonasson, P., Mårtensson, L.-G., & Jonsson, B.-H. (1995) *Biophys. J. 69*, 202−213.

Linske-O'Connell, L. I., Sherman, F., & McLendon, G. (1995) *Biochemistry 34*, 7102−7112.

Lo, T. P., Komar-Panicucci, S., Sherman, F., McLendon, G., & Brayer, G. D. (1995) *Biochemistry 34*, 5259−5268.

Louie, G. V., & Brayer, G. D. (1990) *J. Mol. Biol. 214*, 527−555.

Margoliash, E., & Frohwirt, N. (1959) *Biochem. J. 71*, 570−572.

Marmorino, J. L., & Pielak, G. J. (1995) *Biochemistry 34*, 3140−3143.

Marsh, D. (1989) in *Biological Magnetic Resonance* (Berliner, L. J., & Ruben, J., Eds.) Vol. 8, Chapter 5, pp 255−303, Plenum, New York.
Mascarenhas, R., Wei, Y.-H., Scholes, C. P., & King, T. E. (1983) *J. Biol. Chem. 258*, 5348−5351.
Matsuura, Y., Takano, T., & Dickerson, R. E. (1982) *J. Mol. Biol. 156*, 389−409.
Mchaourab, H. S., Lietzow, M. A., Hideg, K., & Hubbell, W. L. (1996) *Biochemistry 35*, 7692−7704.
Miick, S. M., Todd, A. P., & Millhauser, G. L. (1991) *Biochemistry 30*, 9498−9503.
Moore, G. R., & Pettigrew, G. W. (1990) *Cytochromes c Evolutionary, Structural and Physicochemical Aspects*, pp 49−55, Springer-Verlag, Berlin.
Mulligan-Pullyblank, P., Spitzer, J. S., Gilden, B. M., & Fetrow, J. S. (1996) *J. Biol. Chem. 271*, 8633−8645.
Murphy, M. E. P., Nall, B. T., & Brayer, G. D. (1992) *J. Mol. Biol. 227*, 160−176.
Murphy, M. E. P., Fetrow, J. S., Burton, R. E., & Brayer, G. D. (1993) *Protein Sci. 2*, 1429−1440.
Myer, Y. P. (1985) *Current Topics in Bioenergetics*, Vol. 14, pp 149−188, Academic Press, Inc., New York.
Ochi, H., Hata, Y., Tanaka, N., Kakudo, M., Sakurai, T., Aihara, S., & Morita, Y. (1983) *J. Mol. Biol. 166*, 407−418.
Pace, C. N. (1986) *Methods Enzymol. 131*, 266−280.
Pace, C. N., Shirley, B. A., & Thomson, J. A. (1989) in *Protein Structure: A Practical Approach* (Creighton, T. E., Ed.), pp 311−330, Oxford University Press, Oxford.
Pascher, T., Chesick, J. P., Winkler, J. R., & Gray, H. (1996) *Science 271*, 1558−1560.
Pielak, G. J., Auld, D. S., Beasley, J. R., Betz, S. F., Cohen, D. S., Doyle, D. F., Finger, S. A., Fredericks, Z. L., Hilgen-Willis, S., Saunders, A. J., & Trojak, S. K. (1995) *Biochemistry 34*, 3268−3276.
Roder, H., Elöve, G. A., & Englander, S. W. (1988) *Nature 335*, 700−704.
Santoro, M. M., & Bolen, D. W. (1988) *Biochemistry 27*, 8063−8068.
Schellman, J. A. (1978) *Biopolymers 17*, 1305−1322.
Schmid, F. X. (1992) in *Protein Folding* (Creighton, T. E., Ed.) pp 197−241, W. H. Freeman & Co., New York.
Schneider, D. J., & Freed, J. H. (1989) in *Biological Magnetic Resonance* (Berliner, L. J., & Ruben, J., Eds.) Vol. 8, Chapter 1, pp 1−76, Plenum, New York.
Schweingruber, M. E., Sherman, F., & Stewart, J. W. (1977) *J. Biol. Chem. 252*, 6577−6580.
Sherman, F., Stewart, J. W., Jackson, M., Gilmore, R. A., & Parker, J. H. (1974) *Genetics 77*, 255−284.
Shin, Y.-K., Levinthal, C., Levinthal, F., & Hubbell, W. L. (1993) *Science 259*, 960−963.
Sienkiewicz, A., Qu, K., & Scholes, C. P. (1994) *Rev. Sci. Instrum. 65*, 68−74.
Sosnick, T. R., Mayne, L., Hiller, R., & Englander, S. W. (1994) *Nat. Struct. Biol. 1*, 149−156.
Sosnick, T. R., Mayne, L., & Englander, S. W. (1996) *Proteins 24*, 413−426.
Steinhoff, H., Mollaaghababa, R., Altenbach, C., Hideg, K., Krebs, M., Khorana, H. G., & Hubbell, W. L. (1994) *Science 266*, 105−107.
Takano, T., & Dickerson, R. E. (1980) *Proc. Natl. Acad. Sci. U.S.A. 77*, 6371−6375.
Timkovich, R., & Dickerson, R. E. (1976) *J. Mol. Biol. 251*, 4033−4046.
Todd, A. P., & Millhauser, G. L. (1991) *Biochemistry 30*, 5515−5523.
Todd, A. P., Cong, J., Levinthal, F., & Hubbell, W. F. (1989) *Proteins 6*, 294−305.
Tsong, T. Y. (1976) *Biochemistry 15*, 5467−5473.
Wynn, R., & Richards, F. M. (1993) *Protein Sci. 2*, 395−403.
Zuniga, E. H., & Nall, B. T. (1983) *Biochemistry 22*, 1430−1437.

BI962155I